DALTON
FULL PAPER

Thioether–iodine charge-transfer complexes. Synthesis and low-temperature single-crystal structures of complexes of penta-, hexa- and octa-dentate homoleptic thioether macrocycles

Alexander J. Blake,[a] Francesco A. Devillanova,[b] Alessandra Garau,[b] Liam M. Gilby,[c] Robert O. Gould,[c] Francesco Isaia,[b] Vito Lippolis,[a,b] Simon Parsons,[c] Christian Radek[c] and Martin Schröder*,[a]

[a] *Department of Chemistry, The University of Nottingham, University Park, Nottingham, UK NG7 2RD*
[b] *Dipartimento di Chimica e Tecnologie Inorganiche e Metallorganiche, University of Cagliari, Via Ospedale 72, 09124 Cagliari, Italy*
[c] *Department of Chemistry, The University of Edinburgh, West Mains Road, Edinburgh, UK EH9 3JJ*

Charge-transfer complexes 2([15]aneS$_5$)·7I$_2$ **1** ([15]aneS$_5$ = 1,4,7,10,13-pentathiacyclopentadecane), [18]aneS$_6$·I$_2$ **2**, [18]aneS$_6$·4I$_2$ **3** ([18]aneS$_6$ = 1,4,7,10,13,16-hexathiacyclooctadecane), [24]aneS$_8$·I$_2$ **4** and [24]aneS$_8$·6I$_2$ **5** ([24]aneS$_8$ = 1,4,7,10,13,16,19,22-octathiacyclotetracosane) have been prepared and their structures and solution properties investigated. The compounds were prepared by slow evaporation of solutions containing I$_2$ and the appropriate thioether macrocycle in CH_2Cl_2. The single-crystal structure determination of **1** shows three I$_2$ molecules co-ordinated to three *exo* oriented S donors [S(1)–I(1) 2.797(3), I(1)–I(1′) 2.798(2), S(4)–I(4) 2.885(4), I(4)–I(4′) 2.764(2), S(7)–I(7) 2.828(3) and I(7)–I(7′) 2.779(2) Å; S(1)–I(1)–I(1′) 178.39(8), S(4)–I(4)–I(4′) 171.12(8), S(7)–I(7)–I(7′) 178.80(8)°]. The fourth I$_2$ molecule (with a site occupancy of 0.5) lies close to S(10) [I(10)–S(10) 2.839(5) Å], the bond distance I(10)–I(10′) 2.674(3) Å being unusually short. Compound **2** is an example of a 1:1 I$_2$:macrocycle adduct and shows symmetrically bridging I$_2$ molecules [S(1)–I(1) 3.099(2), I(1)–I(1^i) 2.7881(10) Å; S(1)–I(1)–I(1^i) 178.68(4)°; i $1-x$, $1-y$, $1-z$] between [18]aneS$_6$ macrocycles. Compound **3** is the first example of an adduct between I$_2$ and a homoleptic thioether macrocycle which shows both *exo* [S(1)–I(1) 2.838(2), I(1)–I(1′) 2.7875(6) Å; S(1)–I(1)–I(1′) 174.95(4)°] and *endo* [S(4)–I(4) 2.792(2), I(4)–I(4′) 2.8067(7) Å; S(4)–I(4)–I(4′) 174.43(4)°] co-ordination of I$_2$ molecules. The *endo*-oriented I$_2$ molecules occupy space above and below the macrocyclic plane with the macrocycle adopting a sigmoid conformation. The single-crystal structure determination of the 1:1 adduct **4** shows symmetrically bridging I$_2$ molecules [S(1)–I(1) 3.215(2) and I(1)–I(1^i) 2.758(2) Å; S(1)–I(1)–I(1^i) 172.75(3)°; i $-x$, $-y$, $-z$] which are a characteristic of this stoichiometry. Compound **5** contains *endo*- and *exo*-oriented S donors within the same adduct [I(1)–I(1′) 2.7861(8), I(4)–I(4′) 2.7937(8), I(7)–I(7′) 2.8345(8), S(1)–I(1) 2.821(2), S(4)–I(4) 2.815(2), S(7)–I(7) 2.741(2) Å; S(1)–I(1)–I(1′) 170.15(5), S(4)–I(4)–I(4′) 177.41(5), S(7)–I(7)–I(7′) 177.24(5)°]. These results are discussed in the context of the stability and characteristics of thioether crown–iodine charge-transfer complexes, and a qualitative MO diagram is proposed to account for the shorter I–I distances in bridging I$_2$ fragments compared to those in terminally bound I$_2$.

In 1993 we reported the results of our investigation of charge-transfer complexes of I$_2$ with the tridentate thioether crown [9]aneS$_3$,[1] and have subsequently extended these studies to the tetradentate macrocycles [*n*]aneS$_4$ (*n* = 12, 14, 16).[2–4] We have shown that these complexes exhibit a range of unusual structures in which I$_2$ acts as a template to order the macrocyclic metal receptors in the solid state. Charge-transfer adducts between non-macrocyclic thione, thioether and related donors and I$_2$ are well known.[5–9] However, using macrocyclic thioethers we were able to identify trends which could be correlated with the stoichiometry of the adduct.[2] For example, the bridging of I$_2$ molecules in 1:1 adducts, in which I$_2$ molecules span independent macrocycles to give infinite chain structures, was observed to be either symmetrical with equal S–I distances or asymmetrical with a long and a short S–I distance. The single-crystal structure of, for example, [12]aneS$_4$·I$_2$ features both types of bridging within the same structure.[2,3] For charge-transfer adducts having higher diiodine content three-dimensional assemblies were observed in the solid state, characterised by S···I and I···I secondary interactions. The use of small- to medium-sized macrocycles afforded charge-transfer adducts in which the sulfur lone pairs were, as expected, exo-dentate to the ring. We argued that perhaps larger ionophores might favour macrocyclic in-cavity co-ordination of I$_2$, and report herein the synthesis and structures of the charge-transfer adducts between I$_2$ and the 15-, 18- and 24-membered homoleptic thioether macrocycles [15]aneS$_5$, [18]aneS$_6$ and [24]aneS$_8$.

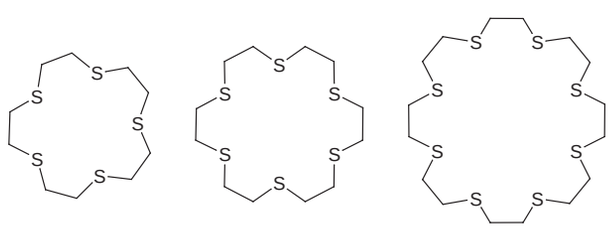

Results and Discussion

Solution studies

Solutions containing I$_2$ and homoleptic thioether macrocycles in CH_2Cl_2 are dark brown, in contrast to the violet solution of

Table 1 Molar absorption coefficients (ε) at the wavelengths (λ) used for the calculation, association constants (*K*), ranges of the saturation fraction (*s*), and sum of the squared deviations (χ^2) for [24]aneS$_8$ (1,4,7,10,13,16,19,22-octathiacyclotetracosane) with I_2. Standard deviations in parentheses

T/°C	λ/nm	ε/dm^3 cm^{-1} mol^{-1}	*K*/dm^3 mol^{-1}	*s*	χ^2
15	340	15 190(221)	333(8)	0.12–0.83	0.15
	330	21 370(324)			
	320	26 680(407)			
	310	29 660(401)			
	300	28 490(424)			
	290	23 960(545)			
20	340	15 090(181)	266(6)	0.10–0.80	0.09
	330	21 090(268)			
	320	26 280(338)			
	310	29 290(320)			
	300	28 270(367)			
	290	23 970(519)			
25	340	14 990(154)	213(5)	0.08–0.76	0.06
	330	20 860(222)			
	320	26 060(285)			
	310	28 970(269)			
	300	28 140(331)			
	290	24 020(510)			
30	340	14 530(135)	179(4)	0.07–0.73	0.05
	330	20 100(200)			
	320	25 040(250)			
	310	27 920(243)			
	300	27 280(316)			
	290	23 520(504)			
35	340	14 770(126)	137(3)	0.06–0.67	0.03
	330	20 330(165)			
	320	25 290(207)			
	310	28 300(183)			
	300	27 860(297)			
	290	24 230(511)			

$\Delta H = -33.6 \pm 0.1$ kJ mol^{-1}; $r = 0.999$; r = correlation coefficient of the plots of ln ($K\varepsilon$) *vs.* $1/T$ obtained for the six wavelengths.

I_2 in CH_2Cl_2. The change of colour confirms the formation of charge-transfer adducts. We have shown that the 1:1 adduct with I_2 is the predominant species in solution under high dilution conditions for all the thioether macrocycles studied including [15]aneS$_5$ and [18]aneS$_6$.[2a] Spectrophotometric studies in solution allowed measurement of the formation constants (*K*) and the thermodynamic parameters for the formation of a charge-transfer adduct, equation (1).

$$D + I_2 \rightleftharpoons D{\cdot}I_2 \qquad (1)$$

The behaviour of [24]aneS$_8$ does not differ from that of the other smaller macrocyclic crown thioethers already studied. Thus, only one isosbestic point at 479 nm [$\lambda_{CT} = 310$ nm, $\varepsilon_{CT} = 28\,970(270)$ dm^3 mol^{-1} cm^{-1}] is observed on recording the electronic spectra of different solutions containing a constant amount of [24]aneS$_8$ and increasing amounts of I_2 up to a [24]aneS$_8$:I_2 molar ratio of 1:5. This suggests that under these dilution conditions only the formation of the 1:1 adduct is relevant; however, in order to avoid the formation of other adducts, all the solutions used for the calculation of the formation constant (*K*) were prepared with the concentration of [24]aneS$_8$ always higher than that of I_2. Table 1 gives the results obtained from the data treatment. The calculated *K* value at 25 °C, 213 dm^3 mol^{-1}, falls in the range of variability (13–827 dm^3 mol^{-1}) observed for other thioether crowns.[2] We have introduced[2a] the mean number of CH_2 groups (*n*) for each sulfur atom as a parameter that could take into account the inductive effects of the thioether atoms (−I) and of the methylene groups (+I) on the values of *K* and Δ*H*. In particular, we found a broadly linear dependence of the Δ*H* values upon *n*, with a high spread of Δ*H* values for all compounds for $n = 2$ (Fig. 1), the only case where more than one macrocyclic ligand was studied. This spread is attributed to solvation effects and to the existence of several potential conformers for each charge-transfer adduct in solution that might play an important role in the observed values of *K* and Δ*H*. As one can see in Fig. 1, [24]aneS$_8$ basically behaves like other macrocyclic crown thioethers. These results underline the relative weakness of the charge-transfer interaction and it seems likely that any complex undergoes at least some dissociation in solution thus rendering solution or matrix techniques (NMR, IR or FAB mass spectroscopy) for characterisation of iodine-rich compounds inappropriate. Indeed, solid-state samples of charge-transfer adducts do lose I_2 over a period of time.

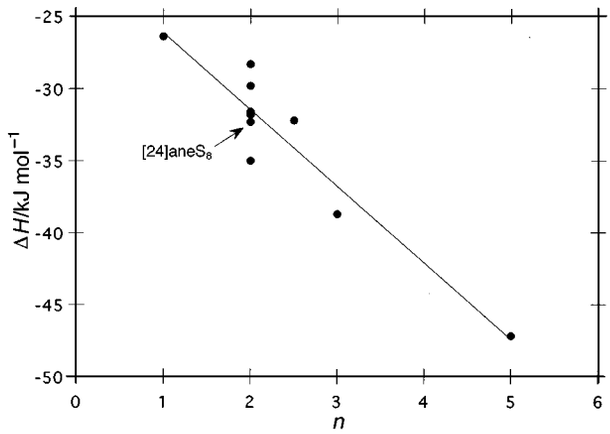

Fig. 1 Plot of Δ*H* *vs.* *n* (*n* = average number of CH_2 groups for sulfur atom) for I_2 adducts with thioether crowns

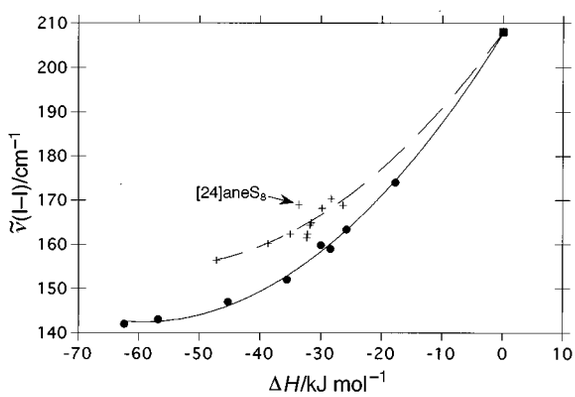

Fig. 2 Plot of ν(I–I) Raman frequencies *vs.* Δ*H* values. The lower curve (●) refers to CH_2Cl_2 solutions of iodine-thioketonic charge-transfer adducts,[2a] the upper curve (+) to CH_2Cl_2 solutions of thioether crown adducts. The value of 208 cm^{-1} (Δ*H* = 0) (■) refers to a CH_2Cl_2 solution of I_2

The FT-Raman spectrum recorded on a CH_2Cl_2 solution of [24]aneS$_8$ and I_2 in 1:0.8 molar ratio shows one broad band in the characteristic ν(I–I) region at 169 cm^{-1} with a band half-width of 18 cm^{-1}. Fig. 2 shows the plot of the ν(I–I) Raman shifts in solution *vs.* values of Δ*H* for all the iodine–thioether crown adducts including [24]aneS$_8$. The plot shows the similarity in behaviour of [24]aneS$_8$ with respect to other macrocycles in their interactions with I_2 in solution, the 1:1 adduct being the predominant species. Table 2 shows the ν(I–I) Raman frequencies recorded on solid samples and the *d*(I–I) bond distances for all the adducts structurally characterised (see below).

The ν(I–I) Raman band, observed at 180 cm^{-1} for I_2 in the solid state,[10] is expected to move to lower frequencies when I_2 interacts with donors to form charge-transfer adducts. Indeed, the interaction with a donor does produce a decrease of I–I bond order, in agreement with a molecular orbital (MO) description,[11] which shows that the highest occupied molecular orbital (HOMO) for the adduct has some degree of σ* I–I antibonding character. In the case of weak or medium-weak

Table 2 Solid-state Raman peaks ν(I–I) and *d*(I–I) bond distances for structurally characterised iodine–thioether crown adducts

Ligand	Adduct	Ref.	ν(I–I)/cm^{-1}	*d*(I–I)/Å
[6]aneS$_2$	[6]aneS$_2$·I$_2$	9	162s, 153ms	2.787(2)
[6]aneS$_3$	[6]aneS$_3$·I$_2$[a]	2(*b*)	171s	2.754(1)
[9]aneS$_3$	2([9]aneS$_3$)·4I$_2$[a]	1(*b*)	171s	2.754(2)
			159ms	2.799(2), 2.785(2). 2.816(2)[b]
	[9]aneS$_3$·3I$_2$	1(*b*)	162	2.772(1), 2.768(2), 2.751(2)[b]
[12]aneS$_4$	[12]aneS$_4$·I$_2$[a]	2(*a*)	170s	2.7549(8), 2.7500(10)[b]
[14]aneS$_4$	[14]aneS$_4$·I$_2$	2(*a*)	155s	2.8095(11)
	[14]aneS$_4$·2I$_2$	2(*a*)	152s	2.821(2), 2.808(2)[b]
	[14]aneS$_4$·4I$_2$	2(*c*)	166s, 157s	2.7571(10), 2.7894(18)
[16]aneS$_4$	[16]aneS$_4$·I$_2$	2(*a*)	165s	2.773(12)
	[16]aneS$_4$·4I$_2$	2(*a*)	156s	2.8108(9), 2.7916(8)[b]
[15]aneS$_5$	2([15]aneS$_5$)·7I$_2$	This work	169s (br)[c]	2.798(2), 2.764(2), 2.779(2)[b]
				2.674(3)[d]
[18]aneS$_6$	[18]aneS$_6$·I$_2$[a]	This work	165s	2.7881(10)
	[18]aneS$_6$·4I$_2$	This work	153s	2.7875(6), 2.8067(7)[b]
[24]aneS$_8$	[24]aneS$_8$·I$_2$[a]	This work	170s	2.758(2)
	[24]aneS$_8$·6I$_2$	This work	171s (br)	2.7861(8), 2.7937(8)[b]
			155 (sh), 147s (br)	2.8345(8)

s = Strong, m = medium, sh = shoulder, br = broad.

[a] Adduct having a diiodine molecule bridging two macrocycle molecules. The compound [18]aneS$_6$·3I$_2$[4] not reported in the table has a bridging I$_2$ molecule (see Table 3). [b] The mean value of the *d*(I–I) bond distances has been used in the linear correlation reported in Fig. 3. [c] The Raman band is broad with a band half-width of 30 cm^{-1} and could contain the contributions of different diiodine molecules. [d] Occurs in a region of disorder and therefore may be unreliable.

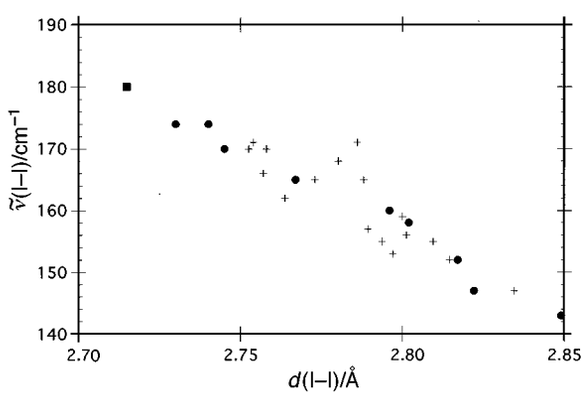

Fig. 3 Correlation between the ν(I–I) Raman frequencies and the bond lengths *d*(I–I): (+) solid iodine–thioether crown adducts, (●) solid charge-transfer complexes of thionic–compounds with I$_2$.[12] The value of 180 cm^{-1} [*d*(I–I) = 2.715(6) Å] (■) refers to solid I$_2$[13]

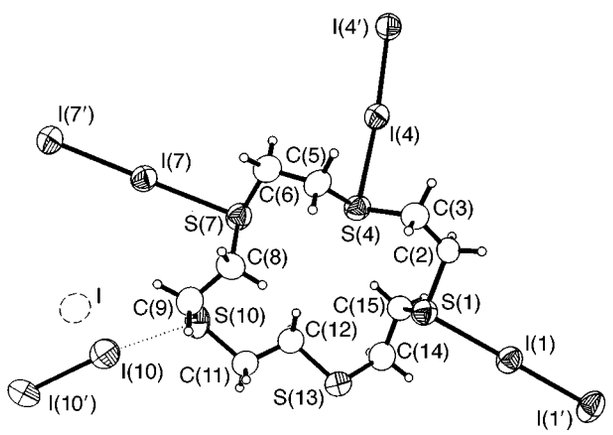

Fig. 4 Single-crystal structure of 2([15]aneS$_5$)·7I$_2$ **1** with numbering scheme adopted. Displacement ellipsoids enclose 50% probability surfaces and hydrogen atoms are drawn with arbitrary radii

adducts (I–I bond order >0.6),[12] for example those involving a sulfur atom as donor, the ν(I–I) Raman frequencies can be roughly correlated to the *d*(I–I) bond distances. Fig. 3 shows a plot of values of ν(I–I) *vs*. *d*(I–I) for the iodine–thioether crown adducts and for some I$_2$ charge-transfer adducts with thionic compounds (Table 2).[12] It is noteworthy that the FT-Raman spectrum of [6]aneS$_2$·I$_2$ is not consistent with structural data reported by Chao and McCullough.[9] In fact the two peaks at 162 and 153 cm^{-1} (Table 2) should coincide with the presence of two I$_2$ molecules having different bond distances; however, the refinement of the crystal structure would not proceed beyond $R = 0.18$ and its resulting imprecision may be the source of this discrepancy.

Structural studies

Crystals of charge-transfer adducts of diffraction quality were grown by evaporation of solvent from solutions of macrocycle and varying concentrations of I$_2$. A single-crystal structure determination of 2[15]aneS$_5$·7I$_2$ **1** reveals a number of features similar to those in 2([9]aneS$_3$)·4I$_2$,[1] which may, in general, be attributed to the odd number of donors within the macrocycles. The asymmetric unit (Fig. 4) contains one [15]aneS$_5$ macrocycle and three I$_2$ molecules co-ordinated to three S donors [S(1)–I(1) 2.797(3), I(1)–I(1′) 2.798(2), S(4)–I(4) 2.885(4), I(4)–I(4′) 2.764(2), S(7)–I(7) 2.828(3) and I(7)–I(7′) 2.779(2) Å; S(1)–I(1)–I(1′) 178.39(8), S(4)–I(4)–I(4′) 171.12(8) and S(7)–I(7)–I(7′) 178.80(8)°]. Although the fourth I$_2$ molecule (with a site occupancy of 0.5) lies a reasonable distance from S(10) [I(10)–S(10) 2.839(5) Å] it shows an I–I bond length [I(10)–I(10′) 2.674(3) Å] shorter than that seen in I$_2$ in the solid state [2.715(6) Å][13] and only marginally longer than that observed for I$_2$ in the vapour phase [2.667(2) Å].[14] Using I–I bond lengths as a sensitive probe for co-ordinative bonding, it has to be concluded that relatively little electron density is transferred into the antibonding LUMO of the I$_2$ molecule. The overlap between a lone pair of S(10) and the antibonding LUMO of this I$_2$ molecule [I(10)–I(10′)] should therefore be poor in order to account for the unexpectedly short I–I bond length. However, the I(10)–S(10) bond distance of 2.839(5) Å might suggest an interaction between the full π*-antibonding orbitals of I$_2$ with an empty acceptor orbital on sulfur. Such interaction could account for the observed I(10)–S(10) and I(10)–I(10′) bond distances with the I$_2$ molecule also behaving as donor. The situation is, however, complicated by the presence of a large residual peak (approximately 12 e Å^{-3}) in close proximity to I(10) [I···I(10) 1.562(6) Å] which has been

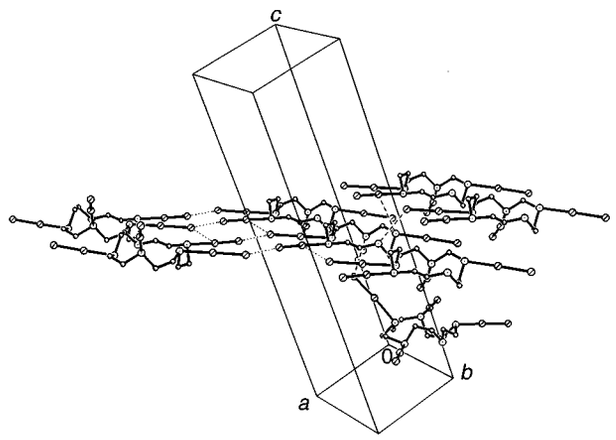

Fig. 5 View of the packing diagram of 2([15]aneS$_5$)·7I$_2$ **1** (hydrogen atoms omitted); I···I contacts are shown as dotted lines and S···I contacts as dashed lines

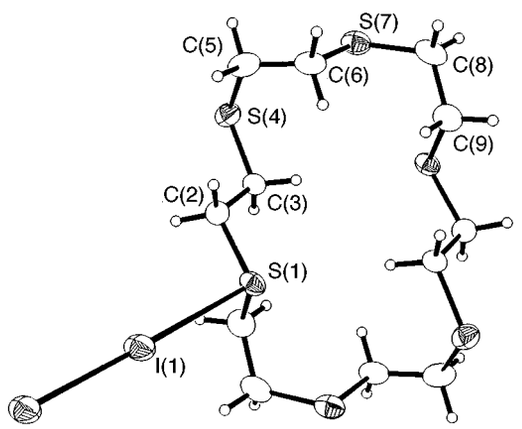

Fig. 6 Single-crystal structure of [18]aneS$_6$·I$_2$ **2** with numbering scheme adopted. Details as in Fig. 4

modelled as an I atom with a site occupancy of 0.2. Its close proximity excludes the possibility of both being present in the same asymmetric unit, and therefore analysis of this region of the structure of this adduct should be treated with caution. Furthermore, the Raman spectroscopy of 2([15]aneS$_5$)·7I$_2$ in the solid state is not helpful in clarifying the nature of the I(10)–I(10′) diiodine molecule since only a unique broad peak at 168 cm^{-1} is observed.

In common with [9]aneS$_3$, [15]aneS$_5$ has an odd number of sulfur atoms in the macrocycle which might account for the difficulties of packing in the crystal lattice. Significantly, the macrocycle adopts an unusual distorted [3336] conformation in this adduct. The packing diagram (Fig. 5) shows two types of interactions between molecules: the dotted lines represent I(7′)···I(10^{i}) (i x, $y-1$, z) and I(7′)···I(10′^{ii}) (ii $2-x$, $-y$, $1-z$) contacts of 3.893(2) and 3.691(2) Å respectively and the dashed lines I(4′)···S(4^{iii}) (iii $-x$, $-\frac{1}{2}+y$, $\frac{1}{2}-z$) contacts of 3.903(3) Å. The former gives rise to two-dimensional sheets of molecules while the latter link these into a three-dimensional network.

The adduct [18]aneS$_6$·I$_2$ **2** continues the series of 1:1 adducts between I$_2$ and homoleptic thioether macrocycles. The structure of **2** (Fig. 6) shows one I$_2$ molecule co-ordinated to one of the S donors in [18]aneS$_6$ with the macrocycle showing 12 out of 18 torsion angles less than 90° in a [22232223] conformation, compared to the [234234] conformation observed for the free macrocycle.[15] The packing diagram (Fig. 7) reveals the familiar picture for 1:1 adducts with an infinite one-dimensional chain structure formed by alternating [18]aneS$_6$ and I$_2$ molecules [S(1)–I(1) 3.099(2) and I(1)–I(1^{i}) 2.7881(10) Å; S(1)–I(1)–I(1^{i}) 178.68(4)°] (i $1-x$, $1-y$, $1-z$). Successive macrocycles are related by the symmetry operation $1+x$, y, $1+z$ so that the chains run parallel to the *ac* face diagonal.

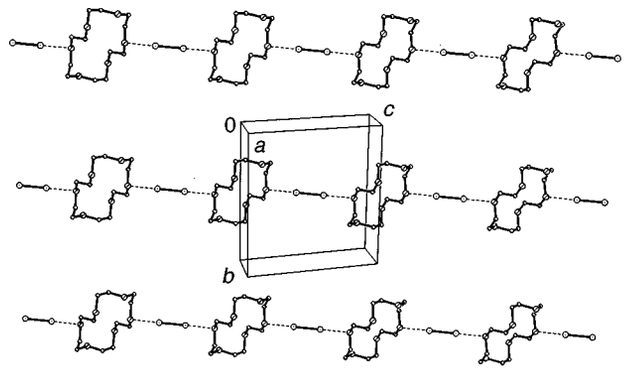

Fig. 7 View of the packing diagram of [18]aneS$_6$·I$_2$ **2** (hydrogen atoms omitted). Macrocycles and I$_2$ molecules alternate within linear chains

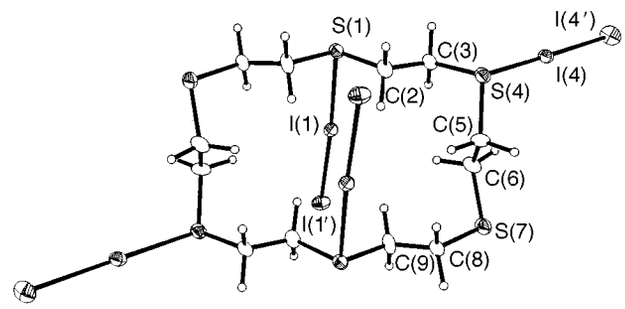

Fig. 8 Single-crystal structure of [18]aneS$_6$·4I$_2$ **3** with numbering scheme adopted. Details as in Fig. 4

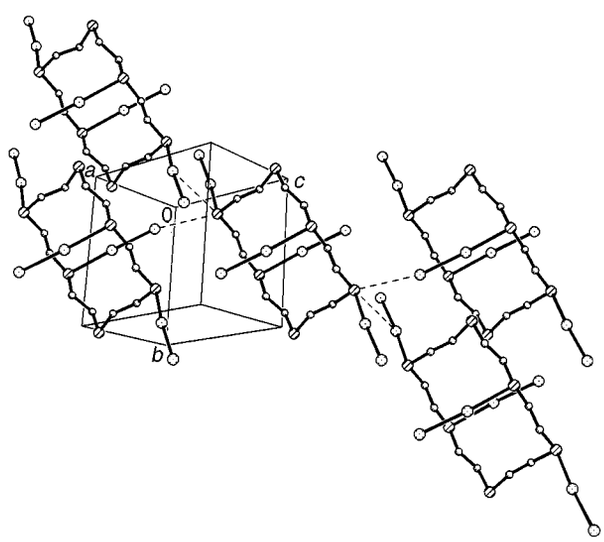

Fig. 9 View of the packing diagram of [18]aneS$_6$·4I$_2$ **3** (hydrogen atoms omitted). A representative part of the three-dimensional lattice formed by I···S contacts (dashed lines) is shown

In the structure of [18]aneS$_6$·4I$_2$ **3** (Fig. 8) the macrocycle adopts a rectangular [2727] conformation. Significantly, two S donors adopt *endo* and four adopt *exo* orientations with *anti* conformations along SCH_2CH_2S moieties. Thus, two I$_2$ molecules adopt typical *exo* co-ordination modes to two S atoms [S(1)–I(1) 2.838(2) and I(1)–I(1) 2.7875(6) Å; S(1)–I(1)–I(1′) 174.95(4)°] with the second pair of *exo* oriented S atoms [S(7) and its symmetry equivalent] remaining uncomplexed. Two *endo* oriented S donors bind to the two remaining

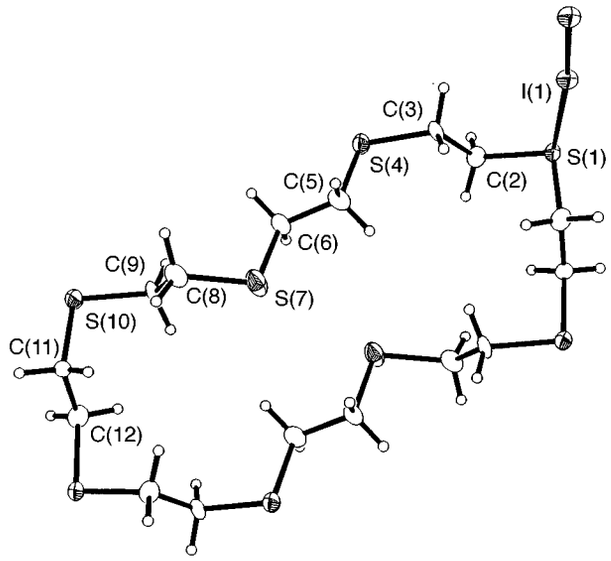

Fig. 10 Single-crystal structure of [24]aneS$_8$·I$_2$ **4** with numbering scheme adopted. Details as in Fig. 4

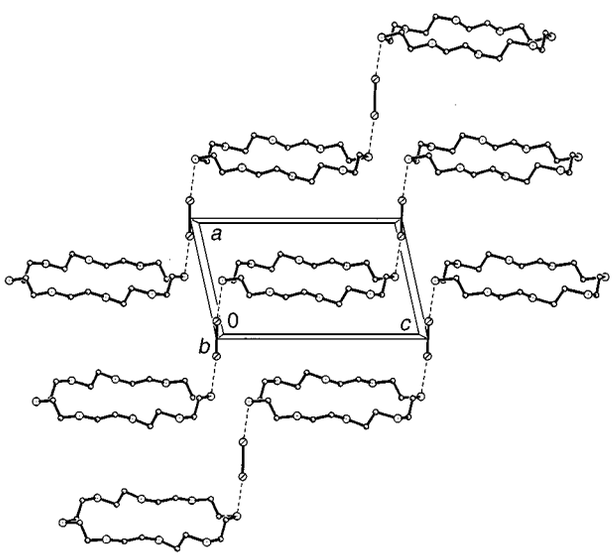

Fig. 11 Packing diagram of [24]aneS$_8$·I$_2$ **4** (hydrogen atoms omitted). In this case the chains of alternating macrocycles and I$_2$ molecules are stepped rather than linear

I$_2$ molecules [S(4)–I(4) 2.792(2) and I(4)–I(4′) 2.8067(7) Å; S(4)–I(4)–I(4′) 174.43(4)°]. The projection used in Fig. 8, approximately onto the least-squares plane through the S atoms, illustrates clearly these two different binding modes. The packing diagram (Fig. 9) shows that molecules of **3** interact through two independent S···I contacts of similar length: S(4)···I(12^{i}) 3.758(3), S(4)···I(41^{ii}) 3.779 Å (i 1 + x, y, z − 1; ii 1 − x, −y, 1 − z) to give a three-dimensional structure.

The adduct [24]aneS$_8$·I$_2$ **4** is the final example in the present investigation of a 1:1 adduct between I$_2$ and a homoleptic thioether macrocycle. The macrocycle [24]aneS$_8$ has formally twice the number of atoms of [12]aneS$_4$ and perhaps unexpectedly this simple analogy extends into the single-crystal structure of **4** (Fig. 10). The structure of [24]aneS$_8$ in **4** can be viewed as linking two [12]aneS$_4$ molecules *via* C(6) and its symmetry equivalent C(6^{ii}) (ii 1 −x, 2 − y, 1 − z). This is also reflected in the conformation of [24]aneS$_8$ [237237] in which SCH$_2$CH$_2$S moieties adopt linear arrangements with six S donors in *exo* and two in *endo* orientations. The solid-state structure of uncomplexed [24]aneS$_8$ has not been reported, although it seems likely that several low energy conformers are possible.[16]

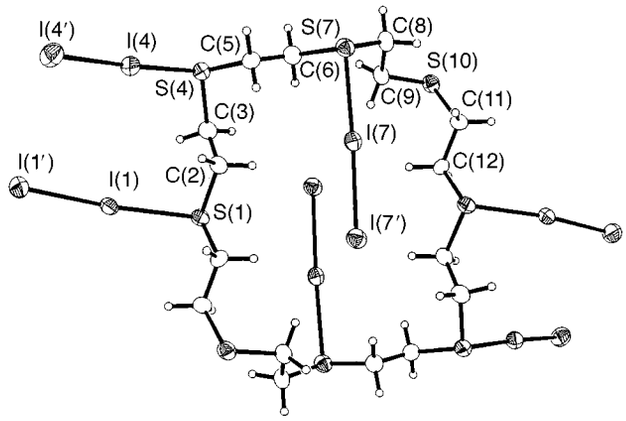

Fig. 12 Single-crystal structure of [24]aneS$_8$·6I$_2$ **5** with numbering scheme adopted. Details as in Fig. 4

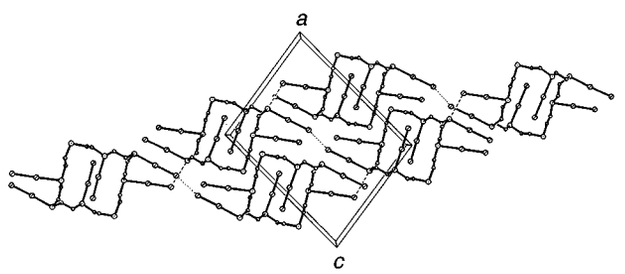

Fig. 13 Packing diagram of [24]aneS$_8$·6I$_2$ **5** (hydrogen atoms omitted). Part of a three-dimensional lattice structure: I···I contacts are shown as dotted lines and S···I contacts as dashed lines

The packing diagram for **4** shows (Fig. 11) the typical one-dimensional chain for 1:1 adducts with symmetrically bridging I$_2$ [S(1)–I(1) 3.215(2) and I(1)–I(1^{i}) 2.758(2) Å, S(1)–I(1)–I(1^{i}) 172.75(3)° (i −x, −y, −z). However, in contrast to the extended structure of **2**, the chains are not linear but form a stair-like arrangement. Successive macrocycles are related by the symmetry operation 1 + x, y, 1 + z so that the chains run parallel to the *ac* face diagonal.

The single-crystal structure of [24]aneS$_8$·6I$_2$ **5** (Fig. 12) shows a centrosymmetric adduct with two I$_2$ molecules bound to *endo* S donors and four I$_2$ molecules bound to the remaining *exo* S donors [S(7)–I(7)–I(7′) 177.24(5), S(1)–I(1)–I(1′) 170.15(5), S(4)–I(4)–I(4′) 177.41(5)°]. The *endo*-bound I$_2$ molecules bend over the macrocycle which, overall, shows an elongated sigmoid conformation. The macrocycle adopts a quasi-rectangular [246246] conformation, similar to that found in **4** which also features 14 *anti* and 10 *gauche* torsion angles. Their environment indicates partial sp^3 hybridisation of the S atoms with C–S–I angles in the range 92.0(3) to 108.6(3)°. The I–I bonds [I(1)–I(1′) 2.7861(8), I(4)–I(4′) 2.7937(8) and I(7)–I(7′) 2.8345(8) Å] are, as expected, elongated due to the S–I interactions [S(1)–I(1) 2.821(2), S(4)–I(4) 2.815(2) and S(7)–I(7) 2.741(2) Å]. Fig. 13 shows part of the infinite, three-dimensional lattice of molecules of **5** linked by S(4)···I(5^{i}) and I(3)···I(3^{ii}) contacts of 3.756(2) and 3.752(2) Å respectively (i 1 + x, $\frac{1}{2}$ − y, $\frac{1}{2}$ + z; ii 1 − x, 1 − y, 1 − z).

Bonding in thioether–iodine CT adducts

A scatter plot of S–I against I–I distances (Fig. 14, Table 3) for a series of thioether/thiocarbonyl complexes with I$_2$ initially shows the close relationship between those two distances.[5] Short S–I distances are associated with long I–I distances and *vice versa*. It is particularly interesting that there is a strong correlation between the type of interaction and the position in the graph. For terminal I$_2$ molecules co-ordinated to thio-

Table 3 Geometrical details of S–I–I moieties in I_2 complexes with some thioether and thicarbonyl ligands

Compound Thioether I_2 complexes	S–I/Å	I–I/Å	S–I–I/°	Ref.
[6]aneS_2·I_2	2.867(6)	2.787(2)	177.9(4)	9
[6]aneS_3·I_2	3.169(1)	2.754(1)	169.04(2)	2(*b*),4
$(PhCH_2)_2S$·I_2	2.78(2)	2.819(9)	179	6(*c*)
Dithia[3.3.1]propellane·$2I_2$	2.852(2)	2.797(1)	*a*	6(*f*)
	2.806(2)	2.797(1)	*a*	
Dithia[3.3.2]propellane·$2I_2$	2.803(2)	2.794(1)	*a*	6(*f*)
	2.902(2)	2.767(1)	*a*	
2(1,10[18]aneS_2O_4)·$5I_2$	2.848(3)	2.775(2)	173.47(7)	6(*c*)
	2.761(3)	2.810(2)	178.03(6)	
	2.774(3)	2.821(2)	175.24(6)	
	2.654(3)	2.902(2)	175.97(7)	
2([9]aneS_3)·$4I_2$	2.792(1)	2.818(1)	174.83(2)	1(*b*)
	2.887(1)	2.781(1)	178.20(2)	
	3.089(1)	2.755(1)	168.86(2)	
	3.239(1)	2.755(1)	176.14(2)	
	2.878(1)	2.792(1)	177.53(3)	
2([9]aneS_3)·$4I_2$	2.870(6)	2.785(2)	178.35(14)	1(*a*),2(*a*)
	2.760(6)	2.816(2)	174.86(14)	
	3.017(6)	2.754(2)	176.18(12)	
	3.054(6)	2.754(2)	168.39(13)	
	2.862(6)	2.799(2)	177.27(14)	
[9]aneS_3·$3I_2$	2.880(3)	2.772(1)	173.5(2)	1(*b*)
	2.865(6)	2.768(2)	175.1(1)	
	2.933(4)	2.751(2)	174.5(1)	
[12]aneS_4·I_2	3.220(3)	2.736(1)	170.5(1)	3
[12]aneS_4·I_2	3.174(2)	2.7549(8)	174.99(4)	2
	3.148(2)	2.7549(8)	170.28(4)	
	3.203(2)	2.7500(10)	165.00(4)	
[14]aneS_4·I_2	2.859(3)	2.8095(11)	178.57(7)	2,4
[14]aneS_4·$2I_2$	2.800(4)	2.821(2)	177.58(8)	2(*a*)
	2.841(4)	2.808(2)	177.86(8)	
[14]aneS_4·$4I_2$	2.803(2)	2.7894(8)	177.71(5)	2(*c*)
	2.880(2)	2.7571(10)	172.50(4)	
[16]aneS_4·I_2	3.114(3)	2.773(12)	173.02(8)	2(*a*)
[16]aneS_4·$4I_2$	2.756(2)	2.8108(9)	174.74(5)	2(*a*)
	2.848(2)	2.7916(8)	171.71(5)	
1 2([15]aneS_5)·$7I_2$	2.797(3)	2.798(2)	178.39(8)	*b*
	2.885(4)	2.764(2)	171.12(8)	
	2.828(9)	2.779(2)	178.80(8)	
2 [18]aneS_6·I_2	3.099(2)	2.7881(10)	178.68(4)	*b*
[18]aneS_6·$3I_2$	2.75	2.8252(9)	178	4
	3.12	2.7725(9)	170	
3 [18]aneS_6·$4I_2$	2.838(2)	2.7875(6)	174.95(4)	*b*
	2.792(2)	2.806(2)	174.43(4)	
4 [24]aneS_8·I_2	3.215(2)	2.758(2)	172.75(3)	*b*
5 [24]aneS_8·$6I_2$	2.821(2)	2.7861(8)	170.15(5)	*b*
	2.815(2)	2.7937(8)	177.41(5)	
	2.741(2)	2.8345(8)	177.24(5)	
Thiocarbonyl I_2 complexes				
Dithizone·I_2	2.664(3)	2.918(1)	178.4(1)	5
Ethylenethiourea·$2I_2$	2.487(3)	3.147(1)	177.9(1)	5
2(Ethylenethiourea)·$3I_2$	2.580(7)	2.984(3)	177.5(2)	5
2(Dithizone)·$7I_2$	2.664(3)	2.918(1)	178.4(1)	5
Ethylenethiourea·I_2 in $(A^+I_3^-)BI_2$ [d]	2.588(8)	2.987(2)	178.2(2)	5(*a*)
5,5-Dimethylimidazolidine-2,4-dithione·I_2	2.748(1)	2.817(1)	176.89(2)	7(*a*)
5,5-Dimethylimidazolidine-2,4-dithione·$2I_2$	2.737(1)	2.849(1)	177.94(4)	7(*a*)
	2.844(1)	2.767(1)	173.74(4)	
5,5-Dimethyl-2-thioxoimidazolidin-4-one·I_2	2.773(1)	2.802(1)	176.14(2)	7(*a*)
N-Methylthiocaprolactam·I_2	2.688(2)	2.880(1)	176.21(4)	8
1,3-Dimethylimidazole-2-thione·I_2	2.616(6)	2.967(12)	175.1(1)	5(*b*)
	2.607(6)	2.984(12)	177.11(4)	
2(Morpholinothiocarbonyl)·$2I_2$	2.920(6)	2.751(2)	175.5(1)	7(*d*)
	2.789(6)	2.805(3)	174.7(1)	
	2.892(6)	2.738(2)	173.9(2)	
	2.801(6)	2.787(3)	176.5(2)	

[a] Value not reported. [b] Present investigation. [c] Dithizone = 1,5-Diphenylthiocarbazone. [d] A = 1-(1-Imidazolin-2-yl)-2-thioxoimidazolidinium, B = ethylenethiourea.

carbonyl S donors, S–I distances lie in the range 2.49 to 2.92 Å and I–I distances from 2.74 to 3.15 Å; for thioether S donors S–I distances occupy the range from 2.65 to 2.93 Å and I–I distances from 2.75 to 2.90 Å. The key to this general behaviour seems to be associated with the stereochemistry of the S donors. Thiocarbonyls are bonded to a single C atom whereas thioethers are bonded to two. The different hybridisation, sp^2 in the case of thiocarbonyls and sp^3 in the case of thioethers, and the

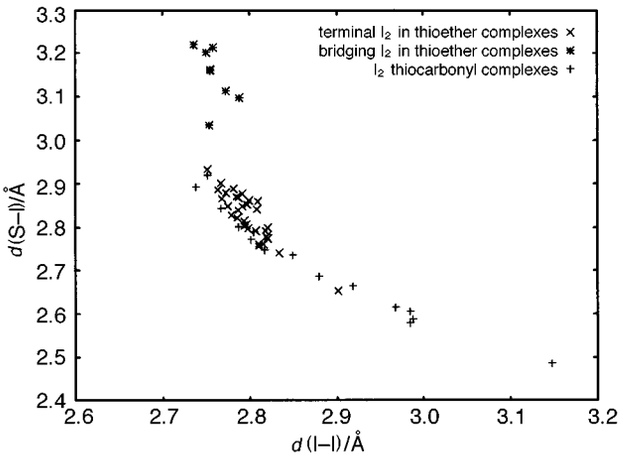

Fig. 14 Scatterplot of I–I against I–S distances for I_2 complexes with some thioether and thiocarbonyl compounds

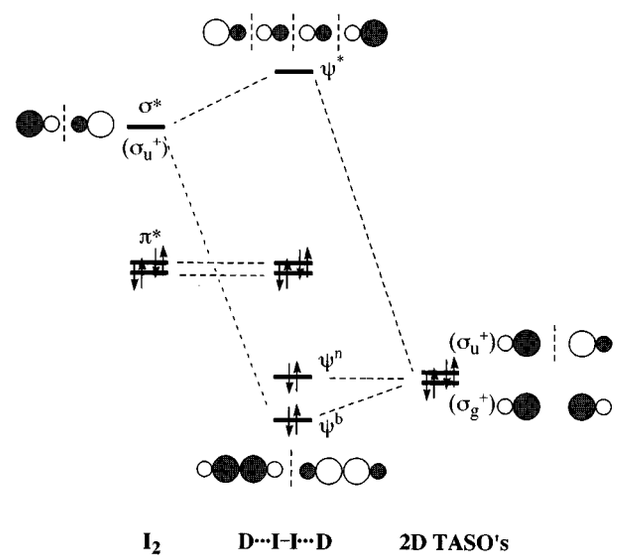

Fig. 15 σ-Only molecular orbital scheme for an idealised $D\cdots I_2\cdots D$ linear symmetric system

associated C–S–I and C–S–C angles of 120° for sp^2 and 109.5° for sp^3 allow more free space around the S donor in case of thiocarbonyls as compared to thioethers thus reducing the effect of packing forces on the molecules. However, for bridging† I_2 molecules in thioether adducts S–I distances lie between 3.10 and 3.22 Å and I–I distances between 2.74 and 2.79 Å. The strong correlation between co-ordination mode and the position in the graph confirms that the division into terminal and bridging I_2 molecules is valid. However, there is no evidence for a subdivision of bridging I_2 molecules into symmetrical and asymmetrical cases. In compounds having both bridging and terminal I_2 molecules, $2([9]aneS_3)\cdot 4I_2$[2a] and $[18]aneS_6\cdot 3I_2$,[4] the former always show shorter I–I distances, and moreover bridging I_2 molecules, in general, are associated with longer S–I distances than terminal I_2 molecules. The magnitude of the elongation of the I–I bond in bridging arrangements is, nevertheless, within the bond length range observed for certain terminal I_2 molecules. The effect of two donors interacting with one I_2 molecule is thus reflected mainly in the longer S–I distances.

Husebye and co-workers[17] have analysed the donor–acceptor interaction between a D–I–I charge transfer unit (D = donor) and another donor (D′) or acceptor (A) by considering the terminal I atom in D–I–I as acting either as a donor or acceptor. Thus, interaction of acceptor A with the terminal I atom in D–I–I will delocalise the negative charge on I leading to a strengthening of the D–I interaction. This is the case of the adducts of the type $D\cdots I_2\cdots I_2$.[18] In contrast, a donor D′ interacting with the same terminal I atom in D–I–I competes with the opposite donor (D) for the diiodine σ* orbital and will lead to a weakening of the D–I interaction. This is the case of a bridging I_2 molecule symmetrically disposed between two donor groups as in $D\cdots I\text{–}I\cdots D$. In these cases it can be concluded that the strong dative influences of the two donors are mutually exclusive and leave the bridging I_2 molecule only slightly perturbed.

An alternative explanation of the longer S–I and shorter I–I bond distances in $D\cdots I_2\cdots D$ systems [as in $[6]aneS_3\cdot I_2$, $2([9]aneS_3)\cdot 4I_2$, $[12]aneS_4\cdot I_2$, $[16]aneS_4\cdot I_2$, $[18]aneS_6\cdot I_2$, $[18]aneS_6\cdot 3I_2$ and $[24]aneS_8\cdot I_2$][2,4] can be based on a simplified MO diagram between the central I_2 molecule and the two donors as shown in Fig. 15. If the $D_{\infty h}$ point group is considered for the symmetry of an idealised $D\cdots I_2\cdots D$ linear symmetric system, the MO scheme shows that of the three MOs ψ^b, ψ^n, ψ^*; only ψ^b contributes to stabilise the system (Fig. 15). The two electrons on ψ^b are however distributed among three bonds rather than between two as in a $D\cdots I_2$ system.[19] This means that each bond in a $D\cdots I_2\cdots D$ system has a lower amount of the ψ^b electron charge than a $D\cdots I_2$ system. Consequently, the $D\cdots I$ bonds in the idealised $D\cdots I_2\cdots D$ system should be longer than in the simple adduct, whereas the I–I bond should be shorter (less ψ^b electron charge is allocated to the σ* molecular orbital of I_2). This explanation should also be valid for the I–I bond distances observed in asymmetric I_3^- ions in comparison with those found in I_4^{2-} ions describable as a linear $[I\cdots I_2\cdots I]^-$ system.[17,19,20]

In contrast to their ease of isolation, the characterisation of the complexes studied has been rather difficult. The problems concerning solution and matrix studies have been addressed above and even microanalysis has proven to be less reliable than, for example, in the case of polyiodide metal complexes of thioether crowns.[21] Contributing to these problems is the weakness of the macrocyclic thioether–iodine interaction, which allows I_2 to sublime off leading to decomposition of samples of the adducts in the solid state. Keeping these points in mind, we were particularly interested to predict in our structural studies the unit cell and especially the I_2 content using the unit-cell volume and the number of formula units Z which can be deduced from the space group. The commonly used '18 $Å^3$ rule' states that the expected unit-cell volume, V, is equal to $18ZN$ where Z is the number of formula units in the unit cell and N is the number of non-hydrogen atoms in the formula unit. However, in the case of macrocyclic I_2 charge-transfer adducts, the value 18 $Å^3$ for an average atomic volume is too small to give accurate results. Using a system of linear equations it was possible to deduce new values for the atomic volumes of C, S and I atoms ($V_C = 23$, $V_S = 24$ and $V_I = 47$ $Å^3$) which were successfully used in predicting the unit-cell contents throughout our investigation. The difference between calculated and measured volumes lies well within a 10% error margin, except for the structure of $2([9]aneS_3)\cdot 4I_2$.

Conclusion

Our present investigation has shown that homoleptic polydentate thioether macrocyclic ligands interact in similar ways with I_2 molecules compared to small mono- or bi-dentate ligands. Features common to both groups of adducts are the quasi-linear S–I–I moieties, the elongation of the I–I bond length compared to I_2 vapour and the close correlation between I–S and I–I bond lengths. The solid-state structures are, as pre-

† For asymmetrically bridged compounds the average of the S–I distances is shown in the plot.

Table 4 Experimental data for single-crystal structure determinations of 2([15]aneS$_5$)·7I$_2$ **1**, [18]aneS$_6$·I$_2$ **2**, [18]aneS$_6$·4I$_2$ **3**, [24]aneS$_8$·I$_2$ **4** and [24]aneS$_8$·6I$_2$ **5**

	1	**2**	**3**	**4**	**5**
Formula	$C_{10}H_{20}I_7S_5$	$C_{12}H_{24}I_2S_6$	$C_{12}H_{24}I_8S_6$	$C_{16}H_{32}I_2S_8$	$C_{16}H_{32}I_{12}S_8$
M	1214.24	614.47	1375.88	734.76	2006.70
Crystal system	Monoclinic	Monoclinic	Triclinic	Monoclinic	Monoclinic
Space group	$P2_1/c$	$P2_1/n$	$P\bar{1}$	$P2_1/a$	$P2_1/c$
a/Å	8.607(5)	5.2783(9)	9.123(3)	9.547(5)	14.784(6)
b/Å	10.100(4)	14.572(2)	9.153(4)	8.599(6)	8.269(4)
c/Å	33.02(2)	13.925(2)	10.408(4)	16.367(12)	18.587(8)
α/°	—	—	82.03(2)	—	—
β/°	92.51(5)	98.14(2)	68.35(2)	102.70(5)	98.73(3)
γ/°	—	—	77.89(3)	—	—
U/Å^3	2867	1060	788	1311	2246
Z	4	2	1	2	2
T/K	150	150	150	150	150
μ/mm^{-1}	8.152	3.547	8.178	3.04	8.66
Measured reflections	5552	2230	2778	1829	4383
Unique reflections, R_{int}	4974, 0.033	1836, 0.104	2665	1685, —	3750, 0.025
Absorption correction range	0.771–1.126	0.316–0.369	0.382–0.648	0.236–0.400	0.098–0.523
Full-matrix least squares on	F^2	F^2	F	F^2	F^2
R, R' [28]	—	—	0.028, 0.039		
$R1$, $wR2$ [29]	0.052, 0.167	0.061, 0.141	—	0.038, 0.158	0.035, 0.126

dicted, rather different and a number of types of interaction such as terminal and bridging as well as *exo* and *endo* co-ordination, have been identified. It would nevertheless be very interesting to continue this area of research focussing, in particular, on three aims. (i) The present investigation has illustrated that an increasing number of donor atoms combined with increasing ring sizes allows I_2 molecules to adopt *endo* co-ordination modes in addition to *exo* co-ordinated I_2 molecules. Extrapolating this trend means that very large ionophores should be able to support bridging I_2 molecules within the macrocyclic cavity. (ii) The plot of S–I against I–I distances contains regions which correlate with particular binding modes. It would be desirable to increase the number of complexes containing bridging I_2 molecules to establish whether this region is in any way connected to the terminal I_2 molecules. An asymmetric bridging I_2 molecule could be viewed as a terminal one with a long-range secondary interaction. We would, therefore, expect that the regions of terminal and bridging I_2 molecules would merge with the growing number of complexes characterised. (iii) The last aim focusses mainly on completing the present investigation. The complexes prepared thus far cover only a fraction of the adducts possible between homoleptic S-donor macrocycles and I_2. It would be interesting to investigate the complete set of adducts formed by varying the proportion of one macrocyclic ligand to I_2, in order to establish trends such as conformational changes of the ligand and packing effects. It seems likely that the more interesting adducts would be with macrocycles possessing odd numbers of S atoms, as it is these which have so far provided the more complex structural features.

Experimental

A typical preparation consisted of mixing solutions of I_2 and the appropriate macrocycle (≈0.05 mmol) in HPLC grade CH_2Cl_2 affording about 15 cm^3 of a dark brown solution. Slow evaporation at room temperature over a period of a few weeks afforded deposits on the glass walls and in the bottom of the reaction vessel. Those deposits appeared in bands which could be distinguished by colour and morphology. It should be noted that most of these deposits occurred as thin films of microcrystals covering the glass walls. Crystalline material suitable for single-crystal X-ray diffraction studies could in general only be recovered from near the bottom of the reaction vessel. The crystallisation products were collected and initially characterised by microanalysis. Larger deviations between observed and calculated values were commonly found for compounds with a high I_2 content, where loss of I_2 was most apparent. Often, however, the microcrystalline deposits found higher up on the glass walls of the reaction vessels showed the same microanalytical and FT-Raman spectra as the crystalline materials collected at the bottom of the reaction vessel. This indicates the formation of the same type of product in high yield in each preparation. {Found: C, 10.81; H, 1.76. Calc. for $C_{10}H_{20}I_7S_5$, 2([15]aneS$_5$)·7I$_2$ **1**: C, 11.87; H, 1.66. Found: C, 10.14; H, 1.29. Calc. for $C_{12}H_{24}I_8S_6$, [18]aneS$_6$·4I$_2$ **3**: C, 10.48; H, 1.76. Found: C, 26.39; H, 4.49. Calc. for $C_{16}H_{32}I_2S_8$, [24]aneS$_8$·I$_2$ **4**: C, 26.15; H, 4.39. Found: C, 10.59; H, 1.70. Calc. for $C_{16}H_{32}I_{12}S_8$, [24]aneS$_8$·6I$_2$ **5**: C, 9.59; H, 1.60%}. The weak nature of the adducts prepared is reflected in the mass spectra which do not show molecular ion peaks for these but only peaks assigned to I_2 and I (m/z = 254 and 127 respectively), the macrocycles and their typical fragmentation products.

Spectrophotometric measurements and data treatment

The spectrophotometric measurements for the determination of the formation constant of the adduct [24]aneS$_8$·I$_2$ were carried out in CH_2Cl_2 solutions using a Varian Cary 5 spectrophotometer having a temperature controller accessory and connected to an IBM PS2 computer. The spectra of 12 different solutions were recorded in the range 250 to 600 nm at temperatures of 15, 20, 25, 30 and 35 °C. The choice of concentrations of the reagents was made according to the criteria outlined and discussed in refs. 22–24. In all the solutions the concentration of [24]aneS$_8$ was always higher than that of I_2 in order to avoid or at least minimise the formation of higher adducts.‡ Data analysis was carried out with a program based on a non-linear least-squares method,[26] assuming that the best values of K and ε are those which minimise the sum of the function $\chi^2 = \Sigma(A_c - A_s)^2/(N - 2)$, where A_c and A_s are the calculated and experimental absorbances and N is the number of data points. The optimisation of K was carried out on six different wavelengths. The value of ΔH and its standard deviation (σ) were calculated by averaging the slopes of the six straight lines obtained by plotting $\ln(K\varepsilon)$ *versus* $1/T$ at six different wave-

‡ The sets of data for [24]aneS$_8$·I$_2$ solutions were analysed using a factor analysis program[25] to determine the number of species present in solution. The presence of only two absorbing species in solution, namely I_2 and the 1 : 1 [24]aneS$_8$·I$_2$ adduct, was confirmed.

Table 5 Selected bond lengths (Å), angles(°) and torsion angles (°) with estimated standard deviations (e.s.d.s) in parentheses for 2([15]aneS$_5$)·7I$_2$ **1**

I···I(10)	1.562(6)	I(10)–I(10′)	2.674(3)
I···I(10′)	2.986(6)	I(1)–S(1)	2.797(3)
I(1)–I(1′)	2.798(2)	I(4)–S(4)	2.885(4)
I(4)–I(4′)	2.764(2)	I(7)–S(7)	2.828(3)
I(7)–I(7′)	2.779(2)	I(10)···S(10)	2.839(5)
I(1′)–I(1)–S(1)	178.39(8)	I(7′)–I(7)–S(7)	178.80(8)
I(4′)–I(4)–S(4)	171.12(8)	I(10′)–I(10)–S(10)	172.90(13)
C(15)–S(1)–I(1)	96.4(4)	C(2)–S(1)–I(1)	99.9(4)
C(3)–S(4)–I(4)	98.6(5)	C(5)–S(4)–I(4)	94.8(5)
C(6)–S(7)–I(7)	97.3(4)	C(8)–S(7)–I(7)	99.2(5)
C(9)–S(10)–I(10)	99.9(5)	C(11)–S(10)–I(10)	120.2(5)

S(1)–C(2)–C(3)–S(4)	−64.9(11)
C(2)–C(3)–S(4)–C(5)	161.9(9)
C(3)–S(4)–C(5)–C(6)	174.9(10)
S(4)–C(5)–C(6)–S(7)	53.7(13)
C(5)–C(6)–S(7)–C(8)	59.5(11)
C(6)–S(7)–C(8)–C(9)	156.9(10)
S(7)–C(8)–C(9)–S(10)	51.8(12)
C(8)–C(9)–S(10)–C(11)	73.2(11)
C(9)–S(10)–C(11)–C(12)	−92.3(11)
S(10)–C(11)–C(12)–S(13)	173.2(7)
C(11)–C(12)–S(13)–C(14)	161.7(10)
C(12)–S(13)–C(14)–C(15)	62.0(12)
S(13)–C(14)–C(15)–S(1)	57.0(12)
C(14)–C(15)–S(1)–C(2)	176.2(9)
C(15)–S(1)–C(2)–C(3)	101.2(10)

Table 6 Selected bond lengths (Å), angles (°) and torsion angles (°) with e.s.d.s in parentheses for [18]aneS$_6$·I$_2$ **2** (i $1-x$, $1-y$, $1-z$; ii $-x$, $1-y$, $-z$)

I(1)–I(1^{i})	2.7881(10)	S(1)–I(1)	3.099(2)
S(1)–I(1)–I(1^{i})	178.68(4)	C(2)–S(1)–I(1)	100.5(2)
C(9^{ii})–S(1)–I(1)	98.3(2)		
S(1)–C(2)–C(3)–S(4)	−174.4(3)	C(6)–S(7)–C(8)–C(9)	64.9(5)
C(2)–C(3)–S(4)–C(5)	68.5(5)	S(7)–C(8)–C(9)–S(1^{ii})	51.0(6)
C(3)–S(4)–C(5)–C(6)	55.3(5)	C(8)–C(9)–S(1^{ii})–C(2^{ii})	170.0(5)
S(4)–C(5)–C(6)–S(7)	58.8(5)	C(9)–S(1^{ii})–C(2^{ii})–C(3^{ii})	−67.4(5)
C(5)–C(6)–S(7)–C(8)	−173.9(4)		

lengths; $\Delta H = (\Sigma \Delta H_i/\sigma_i)/\Sigma 1/\sigma_i$, $\sigma = [(N-1)\Sigma\sigma_i^2/Nn(Nn-1)]^{\frac{1}{2}}$, where N and n are the numbers of the different temperatures and wavelengths respectively. This procedure provides a more reliable value of ΔH than that obtainable by using a van't Hoff plot when the calculated K and ε values are found to be correlated with an observed decrease of ε with increase in temperature.

Raman spectroscopy

The FT-Raman spectra were recorded on a Bruker FRS106 Fourier-transform spectrometer, operating with a diode-pumped Nd:YAG exciting laser (λ = 1064 nm) and having a power tunable up to 350 mW. The InGaAs detector was operated at room temperature; all spectra were recorded at 4 cm^{-1} resolution, down to about 50 cm^{-1} Raman shift. The solid samples were packed into a suitable cell and then fitted into the compartment designed for a 180° scattering geometry. For [24]aneS$_8$ the spectrum in CH_2Cl_2 solution was recorded on a solution of [24]aneS$_8$ and I$_2$ in a 1:0.8 molar ratio ([I$_2$] = 2.6×10^{-2} mol dm^{-3}) contained in a 0.5 cm path length quartz cell.

Crystallography

The following procedure is typical. A single crystal suitable for single-crystal X-ray diffraction studies was mounted in the cold dinitrogen stream of an Oxford Cryosystems low-temperature device[27] on a Stoë Stadi-4 four-circle diffractometer [graphite-monochromated Mo-Kα X-radiation (λ = 0.71 073 Å); ω–2θ scan mode]. Other details of crystal data, data collection and processing and structure analysis are given in Table 4. The single-crystal structures of compounds **3** and **5** were solved by direct methods using SHELXS 86.[28] A Patterson synthesis revealed the positions of the I atoms in the structures of **1**, **2** and **4** using SHELXS 86. The structures were developed by alternating cycles of least-squares refinement and ΔF syntheses. Refinement was on F for **3** using SHELX 76[29] and on F^2 for the others using SHELXL 93.[30] Excessive residual electron density in close proximity to I atoms at isotropic convergence warranted a supplementary empirical absorption correction[31] for compounds **1** and **5**. All non-hydrogen atoms were refined with anisotropic thermal parameters. Hydrogen atoms were included in calculated positions riding on their parent C atoms. Their thermal parameters were either refined with a common

Table 7 Selected bond lengths (Å), angles (°) and torsion angles (°) with e.s.d.s in parentheses for [18]aneS$_6$·4I$_2$ **3** (i $-x$, $1-y$, $-z$)

I(1)–I(1′)	2.7875(6)	I(4)–I(4′)	2.8067(7)
I(1)–S(1)	2.838(2)	I(4)–S(4)	2.792(2)
I(1′)–I(1)–S(1)	174.95(4)	I(4′)–I(4)–S(4)	174.43(4)
I(1)–S(1)–C(2)	98.4(2)	I(4)–S(4)–C(3)	99.0(2)
I(1)–S(1)–C(9^{i})	98.1(2)	I(4)–S(4)–C(5)	106.8(2)
S(1)–C(2)–C(3)–S(4)	176.0(3)	C(6)–S(7)–C(8)–C(9)	70.0(5)
C(2)–C(3)–S(4)–C(5)	70.7(5)	S(7)–C(8)–C(9)–S(1^{i})	−175.2(3)
C(3)–S(4)–C(5)–C(6)	51.7(6)	C(8)–C(9)–S(1^{i})–C(2^{i})	−166.5(5)
S(4)–C(5)–C(6)–S(7)	167.4(4)	C(9)–S(1^{i})–C(2^{i})–C(3^{i})	179.2(5)
C(5)–C(6)–S(7)–C(8)	65.4(5)		

Table 8 Selected bond lengths (Å), angles (°) and torsion angles (°) with e.s.d.s in parentheses for [24]aneS$_8$·I$_2$ **4** (i $-x$, $-y$, $-z$; ii $1-x$, $2-y$, $1-z$)

I(1)–I(1^{i})	2.758(2)	S(1)–I(1)	3.215(2)
S(1)–I(1)–I(1^{i})	172.75(3)	I(1)–S(1)–C(12^{ii})	85.8(2)
I(1)–S(1)–C(2)	107.5(2)		
S(1)–C(2)–C(3)–S(4)	−174.0(3)	S(7)–C(8)–C(9)–S(10)	168.8(3)
C(2)–C(3)–S(4)–C(5)	105.8(5)	C(8)–C(9)–S(10)–C(11)	−75.9(5)
C(3)–S(4)–C(5)–C(6)	−169.9(5)	C(9)–S(10)–C(11)–C(12)	−78.5(5)
S(4)–C(5)–C(6)–S(7)	−178.7(3)	S(10)–C(11)–C(12)–S(1^{ii})	173.0(3)
C(5)–C(6)–S(7)–C(8)	146.1(5)	C(11)–C(12)–S(1^{ii})–C(2^{ii})	−79.1(5)
C(6)–S(7)–C(8)–C(9)	70.6(5)	C(12)–S(1^{ii})–C(2^{ii})–C(3^{ii})	−86.8(5)

Table 9 Selected bond lengths (Å), angles (°) and torsion angles (°) with e.s.d.s in parentheses for [24]aneS$_8$·6I$_2$ **5** (i $-x$, $1-y$, $-z$)

I(1)–I(1′)	2.7861(8)	I(1)–S(1)	2.821(2)
I(4)–I(4′)	2.7937(8)	I(4)–S(4)	2.815(2)
I(7)–I(7′)	2.8345(8)	I(7)–S(7)	2.741(2)
I(1′)–I(1)–S(1)	170.15(5)	I(4)–S(4)–C(5)	98.0(3)
I(1)–S(1)–C(12^{i})	92.0(3)	I(7′)–I(7)–S(7)	177.24(5)
I(1)–S(1)–C(2)	97.9(3)	I(7)–S(7)–C(6)	103.7(3)
I(4′)–I(4)–S(4)	177.41(5)	I(7)–S(7)–C(8)	95.6(3)
I(4)–S(4)–C(3)	108.6(3)		

S(1)–C(12^{i})–C(11^{i})–S(10^{i})	−173.6(4)
C(2)–S(1)–C(12^{i})–C(11^{i})	176.1(6)
C(3)–C(2)–S(1)–C(12^{i})	−173.7(6)
S(4)–C(3)–C(2)–S(1)	157.3(5)
C(5)–S(4)–C(3)–C(2)	47.6(7)
C(6)–C(5)–S(4)–C(3)	76.0(7)
S(7)–C(6)–C(5)–S(4)	−176.2(4)
C(8)–S(7)–C(6)–C(5)	−178.7(6)
C(9)–C(8)–S(7)–C(6)	−46.4(7)
S(10)–C(9)–C(8)–S(7)	−153.6(4)
C(11)–S(10)–C(9)–C(8)	78.2(6)
C(12)–C(11)–S(10)–C(9)	79.8(6)

U_{iso} [0.0495, 0.030 and 0.044 Å^2 in compounds **3**, **4** and **5** respectively] or set at 1.2 times the isotropic U_{eq} value of the parent C atom (in **1** and **2**). Tables 5 to 9 list selected bond lengths, angles and torsion angles. Illustrations were generated using SHELXTL PC,[32] and molecular geometry calculations utilised CALC,[33] SHELXTL PC and SHELXL 93.[30]

CCDC reference number 186/965.

Acknowledgements

We thank EPSRC (UK) and the Consiglio Nazionale delle Ricerche (Italy) for financial support, and the EPSRC Mass Spectrometry Service (University of Swansea) for mass spectra.

References

1 (*a*) A. J. Blake, R. O. Gould, C. Radek and M. Schröder, *J. Chem. Soc.*, *Chem. Commun.*, 1993, 1191; (*b*) F. Cristiani, F. A. Devillanova, F. Isaia, V. Lippolis, G. Verani and F. Demartin, *Heteroatom Chem.*, 1993, **4**, 571.

2 (*a*) A. J. Blake, F. Cristiani, F. A. Devillanova, A. Garau, L. M. Gilby, R. O. Gould, F. Isaia, V. Lippolis, S. Parsons, C. Radek and M. Schröder, *J. Chem. Soc.*, *Dalton Trans.*, 1997, 1337 and refs. therein; (*b*) M. Arca, F. Cristiani, F. A. Devillanova, A. Garau, F. Isaia, V. Lippolis, G. Verani and F. Demartin, *Polyhedron*, 1997, **16**, 1983; (*c*) A. J. Blake, W.-S. Li, V. Lippolis and M. Schröder, *Acta Crystallogr.*, *Sect. C*, 1997, **53**, 886; (*d*) F. Cristiani, F. A. Devillanova, A. Garau, F. Isaia, V. Lippolis, G. Verani, F. Demartin, A. J. Blake, R. O. Gould, C. Radek and M. Schröder, *Synth. Methodologies Inorg. Chem.*, 1994, **4**, 406.

3 P. K. Baker, S. D. Harris, M. C. Durrant, D. L. Hughes and R. L. Richards, *Acta Crystallogr.*, *Sect. C*, 1995, **51**, 697.

4 H. Bock, N. Nagel and A. Seibel, *Liebig Ann. Recl.*, 1997, 2151.

5 (*a*) F. H. Herbstein and W. Schwotzer, *J. Am. Chem. Soc.*, 1984, **106**, 2367; (*b*) F. Freeman, J. W. Ziller, H. N. Po and M. C. Keindl, *J. Am. Chem. Soc.*, 1988, **110**, 2586.

6 (*a*) C. Rømming, *Acta Chem. Scand.*, 1960, **14**, 2145; (*b*) G. Allegra, G. E. Wilson, jun., E. Benedetti, C. Pedone and R. Albert, *J. Am. Chem. Soc.*, 1970, **92**, 4002; (*c*) A. L. Tipton, M. C. Lonergan, C. L. Stern and D. F. Shriver, *Inorg. Chim. Acta*, 1992, **201**, 23; (*d*) J. D. McCullough, G. Y. Chao and D. E. Zuccaro, *Acta Crystallogr.*, 1959, **12**, 815; (*e*) F. H. Erbstein, P. Ashkenazi, M. Kaftory, M. Kapon, G. M. Reisner and D. Ginsburg, *Acta Crystallogr.*, *Sect. B*, 1986, **42**, 575.

7 (*a*) F. Cristiani, F. Demartin, F. A. Devillanova, F. Isaia, G. Saba and G. Verani, *J. Chem. Soc.*, *Dalton Trans.*, 1992, 3553; (*b*) F. Bigoli, P. Deplano, M. L. Mercuri, A. Pellinghelli, A. Sabatini, E. F. Trogu and A. Vacca, *J. Chem. Soc.*, *Dalton Trans.*, 1996, 3583; (*c*) F. Bigoli, P. Deplano, M. L. Mercuri, M. A. Pellinghelli, A. Sabatini, E. F. Trogu and A. Vacca, *Can. J. Chem.*, 1995, **73**, 380; (*d*) D. Atzei, P. Deplano, E. F. Trogu, F. Bigoli, M. A. Pellinghelli and A. Vacca, *Can. J. Chem.*, 1988, **66**, 1481.

8 E. L. Ahlsen and K. O. Strømme, *Acta Chem. Scand.*, *Ser. A*, 1974, **28**, 175.

9 G. Y. Chao and J. D. McCullough, *Acta Crystallogr.*, 1960, **13**, 727.

10 A. Anderson and T. S. Sun, *Chem. Phys. Lett.*, 1970, **6**, 611.

11 K. F. Purcell and J. C. Kotz, *Inorganic Chemistry*, Sanders, Philadelphia, 1997.

12 P. Deplano, F. A. Devillanova, J. R. Ferraro, F. Isaia, V. Lippolis and M. L. Mercuri, *Appl. Spectrosc.*, 1992, **11**, 1625.

13 F. van Bolhuis, P. B. Koster and T. Migchelsen, *Acta Crystallogr.*, 1967, **23**, 90.

14 I. L. Karle, *J. Chem. Phys.*, 1955, **23**, 1739.

15 R. E. Wolf, jun., J. R. Hartman, J. M. E. Storey, B. M. Foxman and S. R. Cooper, *J. Am. Chem. Soc.*, 1987, **109**, 4328.

16 R. Blom, D. W. H. Rankin, H. E. Robertson and M. Schröder, *J. Chem. Soc.*, *Perkin Trans. 2*, 1991, 773; A. J. Blake, M. A. Halcrow and M. Schröder, *Acta Crystallogr.*, *Sect. B*, 1993, **49**, 773.

17 M. D. Rudd, S. V. Lindeman and S. Husebye, *Acta Chem. Scand.*, 1997, **51**, 689.

18 F. Cristiani, F. Demartin, F. A. Devillanova, F. Isaia, V. Lippolis and G. Verani, *Polyhedron*, 1995, **14**, 2937.

19 G. A. Landrum, N. Goldberg and R. Hoffmann, *J. Chem. Soc.*, *Dalton Trans.*, 1997, 3605.

20 F. Bigoli, F. Demartin, P. Deplano, F. A. Devillanova, F. Isaia, V. Lippolis, M. L. Mercuri, M. A. Pellinghelli and E. F. Trogu, *Inorg. Chem.*, 1996, **35**, 3195.

21 A. J. Blake, R. O. Gould, S. Parsons, C. Radek and M. Schröder, *Angew. Chem.*, *Int. Ed. Engl.*, 1995, **34**, 2374; A. J. Blake, V. Lippolis, S. Parsons and M. Schröder, *Chem. Commun.*, 1996, 2207; A. J. Blake, R. O. Gould, W.-S. Li, V. Lippolis, S. Parsons, C. Radek and M. Schröder, *Angew. Chem.*, *Int. Ed. Engl.*, 1998, **37**, 293; A. J. Blake, F. A. Devillanova, R. O. Gould, W.-S. Li, V. Lippolis, S. Parsons, C. Radek and M. Schröder, *Chem. Soc. Rev.*, 1998, in the press.

22 F. A. Devillanova and G. Verani, *Tetrahedron*, 1979, **35**, 511.

23 G. Carta, G. Crisponi and V. Nurchi, *Tetrahedron*, 1981, **37**, 2115.

24 G. Carta and G. Crisponi, *J. Chem. Soc.*, *Perkin Trans. 2*, 1982, 53.

25 H. Gampp, M. Maeder, C. J. Meyer and A. Zuberbühler, *Talanta*, 1985, **32**, 95.

26 G. Crisponi and V. Nurchi, *J. Chem. Educ.*, 1989, **66**, 54.

27 J. Cosier and A. M. Glazer, *J. Appl. Crystallogr.*, 1986, **19**, 105.

28 G. M. Sheldrick, SHELXS 86, *Acta Crystallogr.*, *Sect. A*, 1990, **46**, 467.

29 G. M. Sheldrick, SHELX 76, University of Cambridge, 1976.

30 G. M. Sheldrick, SHELXL 93, University of Göttingen, 1993.

31 N. Walker and D. Stuart, DIFABS, program for applying empirical absorption corrections, *Acta Crystallogr.*, *Sect. A*, 1983, **39**, 158.

32 G. M. Sheldrick, SHELXTL PC, version 4.3. Siemens Analytical X-Ray Instruments., Madison, WI, 1992.

33 R. O. Gould and P. Taylor, CALC, program for molecular geometry calculations, The University of Edinburgh, 1985.

Received 11*th February* 1998; *Paper* 8/01195H